# Comparative Crystal Chemistry of Perovskite-to-Postperovskite Transitions in Germanates under High Pressure

Postperovskite with the $CaIrO_3$ structure in (Mg, Fe)$SiO_3$ characterizes the D″ layer in the lowermost mantle of the Earth. Because of the scarcity of examples of postperovskites in analogue compounds, it is difficult to investigate the criteria for crystallization of the postperovskite structure. One solution is to explain the transition to the $CaIrO_3$-type postperovskite structure by the extrapolated compressive behavior of the $GdFeO_3$-type orthorhombic perovskite. Therefore, we conducted in situ X-ray diffraction experiments to follow the structural change of germanate perovskites. Based on the crystallographic data of $AGeO_3$ (A = Mn, Zn, and Mg), we developed a comparative crystal chemistry approach to stabilize the $CaIrO_3$ structure.

Postperovskite phase transition to the $CaIrO_3$-type structure in magnesium silicates characterizes the structure of the D″ layer in the lowermost mantle of the Earth [1]. Although the change in density for the perovskite-to-postperovskite transition is less than a few percent, the structural change from a corner sharing framework to a layered structure explains the anisotropy in the seismic data of the D″ layer.

Since postperovskite has been found in $MgSiO_3$, many $ABO_3$ compounds have been tested for transformation to the postperovskite phase. However, it is difficult to investigate the criteria for transformation to the $CaIrO_3$-type structure. One of the reasons is that the $CaIrO_3$ structure is not a typical structure of most $ABO_3$ perovskites, except for the related compounds of $CaIrO_3$, such as $CaRhO_3$ [2], $CaPtO_3$ [3], and $CaRuO_3$ [4]. In fact, postperovskites are not found in silicate except for $MgSiO_3$. Moreover, titanate perovskites, such as $FeTiO_3$ [5], $MnTiO_3$ [6], $CaTiO_3$ [7], and $ZnTiO_3$ [8], prefer to decompose to dense oxide compounds rather than to crystallize in the $CaIrO_3$ structure. However, multiple germanate compounds have been reported to crystallize in the $CaIrO_3$ structure. Perovskite–postperovskite transitions of $MgGeO_3$ [9] and $MnGeO_3$ [10] have been confirmed to occur at 55 and 65 GPa. Recently, using the in situ X-ray diffraction method with a laser-heated diamond anvil cell, we found that the perovskite–postperovskite transition in $ZnGeO_3$ occurs above 110–130 GPa [11]. Considering the similarity of the cationic radius of $Zn^{2+}$ with those of $Mg^{2+}$ and $Mn^{2+}$, the transition pressure was unexpectedly high compared with the transition pressure in other germanate compounds.

Theoretical calculations suggest that distortion of $GdFeO_3$-type orthorhombic perovskite could trigger the postperovskite transition [12]. It is well-known that the Goldschmidt tolerance factor represents the distortion in $ABO_3$ perovskites [13]. However, the tolerance factor based on the ionic radii only reflects the distortion at atmospheric pressure. Because the orthorhombic distortion is derived from the rotation of the $BO_6$ octahedra, the rotation angle $\Phi$, which is calculated from the lattice parameters as $\Phi = \cos^{-1}(\sqrt{2}c^2/ab)$, is a useful indicator of the distortion to the postperovskite transition [14]. Our recent studies of fluoride perovskite with sodium fluorides, such as $NaCoF_3$, $NaNiF_3$ and $NaZnF_3$, indicated that the transition starts at $\Phi_{tr}$ = 24–27°. Irrespective of the octahedral constituent cations, other known postperovskites in $MgSiO_3$ and $MgGeO_3$ also

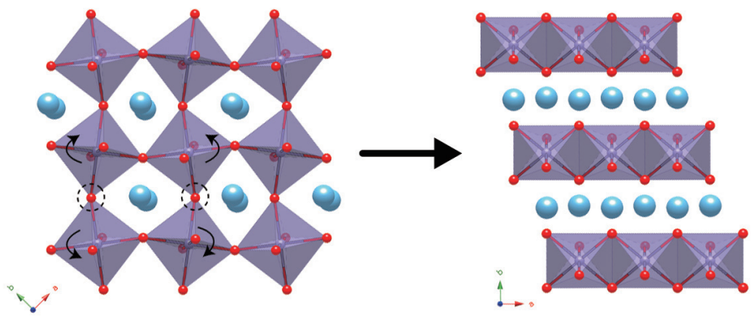

Figure 1: Schematic illustrations of the phase transition from the perovskite (left) to the postperovskite phase (right).

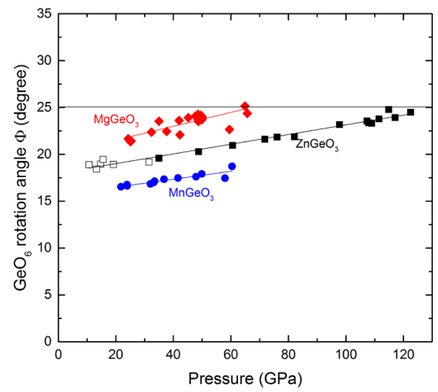


Figure 2: $GeO_6$ rotation angle ($\Phi$) in perovskites as a function of pressure. Diamonds, squares, and circles represent the $\Phi$ values of $MgGeO_3$, $ZnGeO_3$, and $MnGeO_3$, respectively.

exhibit a transition at around $\Phi_{tr}$ = 25°. The above example suggests that $\Phi_{tr} \approx 25°$ would be a critical angle to induce the phase transition to postperovskite. The transformation scheme is shown in Fig. 1. To examine the $\Phi$ value in the present germanate compositions, the lattice parameters of the perovskite and postperovskite phases of $ZnGeO_3$ and $MnGeO_3$ were determined under high pressure with careful annealing with a laser beam to reduce the full-width at half maximum of the X-ray diffraction peaks. Figure 2 shows $\Phi$ of $ZnGeO_3$ and $MnGeO_3$ with pressure change. In this figure, $\Phi$ of $MgGeO_3$, which is calculated from literature data [15], is included for comparison. The gradient of $\Phi$ is almost independent of the divalent cation species. Interestingly, $\Phi_{tr}$ of $ZnGeO_3$ is also located at around $\Phi_{tr}$ = 25°. Therefore, a rather high transition pressure in $ZnGeO_3$ is reasonable with respect to the rotation of the $GeO_6$ octahedra. Instead, according to $\Phi_{tr}$, the low value of $MnGeO_3$ ($\Phi_{tr}$ = 18°) might be an exception. The ionic radius of $Mn^{2+}$ (0.96 Å) is significantly larger than the radii of $Mg^{2+}$ (0.89 Å) and $Zn^{2+}$ (0.90 Å). Therefore, in perovskites with large divalent cations, the corner-sharing $GeO_6$ frameworks cannot generate sufficient space to incorporate the cations by increasing the tilting angle. These frameworks likely decompose to form the postperovskite structure without a large rotation of the $GeO_6$ octahedra. Furthermore, in view of the geometry of the $CaIrO_3$ structure, the *b* axis should be the most sensitive to the divalent cationic radius because divalent cations incorporate into the $GeO_6$ layered structure. In fact, the *b* axis of $MnGeO_3$ is considerably longer than the *b* axes of other germanates. This can be attributed to the ability of the postperovskite structure to incorporate large divalent cations.

## REFERENCES

[1] M. Murakami, K. Hirose, K. Kawamura, N. Sata, and Y. Ohishi, *Science* **304**, 855 (2004).
[2] Y. Shirako, H. Kojitani, M. Akaogi, K. Yamaura, and E. T. -Muromachi, *Phys. Chem. Miner.* **36**, 455 (2009).
[3] K. Ohgushi, Y. Matsushita, N. Miyajima, Y. Katsuya, M. Tanaka, F. Izumi, H. Gotou, Y. Ueda, and T. Yagi, *Phys. Chem. Miner.* **35**, 189 (2008).
[4] H. Kojitani, Y. Shirako, and M. Akaogi, *Phys. Earth Planet. Inter.* **165**, 127 (2007).
[5] D. N. -Hamane, M. G. Zhang, T. Yagi, and Y. M. Ma, *Am. Mineral.* **97**, 568 (2012).
[6] T. Okada, T. Yagi, and D. N. -Hamane, *Phys. Chem. Miner.* 38, 251 (2011).
[7] D. Hamane and T. Yagi, *Review of High Pressure Science and Technology* **22**, 246 (2012).
[8] M. Akaogi, K. Abe, H. Yusa, H. Kojitani, D. Mori, and Y. Inaguma, *Phys. Chem. Miner.* **42**, 421 (2015).
[9] E. Ito, D. Yamazaki, T. Yoshino, H. Fukui, S. M. Zhai, A. Shatzkiy, T. Katsura, Y. Tange, and K. Funakoshi, *Earth. Planet. Sci. Lett.* **293**, 84 (2010).
[10] D. Yamazaki, E. Ito, T. Katsura, T. Yoshino, S. M. Zhai, H. Fukui, A. Shatskiy, X. Z. Guo, S. M. Shan, T. Okuchi, Y. Tange, Y. Higo, and K. Funakoshi, *Am. Mineral.* **96**, 89 (2011).
[11] H. Yusa, T. Tsuchiya, M. Akaogi, H. Kojitani, D. Yamazaki, N. Hirao, Y. Ohishi, and T. Kikegawa, *Inorg. Chem.* **53**, 11732 (2014).
[12] T. Tsuchiya, J. Tsuchiya, K. Umemoto, and R. M. Wentzcovitch, *Earth. Planet. Sci. Lett.* **224**, 241 (2004).
[13] V. M. Goldschmidt, *Naturwissenschaften* **14**, 477 (1926).
[14] M. O'keeffe, B. G. Hyde, and J. O. Bovin, *Phys. Chem. Miner.* **4**, 299 (1979).
[15] C. E. Runge, A. Kubo, B. Kiefer, Y. Meng, V. B. Prakapenka, G. Shen, R. J. Cava, and T. S. Duffy, *Phys. Chem. Miner.* **33**. 699 (2006).

## BEAMLINE

AR-NE1A

**H. Yusa[1] and T. Kikegawa[2] ([1]NIMS, [2]KEK-IMSS-PF)**